U.S. DEPARTMENT OF THE INTERIOR
U.S. GEOLOGICAL SURVEY

PRELIMINARY GEOMAGNETIC PALEOINTENSITIES FROM LONG VALLEY CALDERA, CALIFORNIA

by

Edward A. Mankinen[1]

Open-File Report 94-633

[1]U.S. Geological Survey, Menlo Park, CA

1994

TABLE OF CONTENTS

INTRODUCTION

Paleointensities are being determined in order to characterize geomagnetic intensity variations during Quaternary time. Because the geomagnetic field acts as a shield against cosmic radiation, its intensity directly affects the production rate of radiocarbon (^{14}C) in the upper atmosphere. Coe and others (1978) showed that the variation in dipole moment during Holocene time is nearly proportional to the difference between ^{14}C and tree-ring age. The ^{14}C timescale is currently well calibrated to about 9000 years B.P., and tentatively to about 13,000 years B.P., by comparison with tree-ring and glacial-varve chronologies (Stuiver and others, 1986). However, a comparison of ages determined by the ^{14}C and ^{234}U-^{230}Th methods on coral samples off the island of Barbados (Bard and others, 1990) showed that U-Th ages were consistently older than ^{14}C ages in material older than about 9,000 years. The discrepancy is so large (3,500 years at 25,000 years B.P.) that Bard and others consider that it can only be due to a significant decrease in geomagnetic intensity during the last glacial period. Dipole field intensity has a similar modulating effect on the production of other cosmogenic nuclides that are used for geochronologic studies and will also affect their calibration curves.

Mankinen and Champion (1993*a*,*b*) recently established broad trends in geomagnetic paleointensity for latest Pleistocene and Holocene time on Hawaii. The current study is the beginning of an effort to establish a similar record for western North America. Data from North America and Hawaii will eventually be averaged with other data from globally distributed locations to eliminate the effects on nondipole variations so that a true picture of the global (dipole) field can be obtained. The dipole variations can then be used to model accurately the production rate of cosmogenic nuclides as has been attempted by Mazaud and others (1991, 1994) using some relative paleointensity records from marine sediment cores.

SAMPLES AND AGES

Samples used are from basalt and trachyandesite lava flows of the Long Valley caldera, California on the east side of the Sierra Nevada near Mammoth Lakes. These young lavas erupted in the west moat of the caldera and flowed around the western edge of the resurgent dome and into the north and south moats. The volcanic rocks are part of the Mono-Inyo Craters volcanic chain whose origin may be in magma chambers unrelated to the main Long Valley silicic chamber (Bailey, 1989). Details of the geology, geochronology, and paleomagnetism of these rocks are described in Bailey and others (1976), Mankinen and others (1986), and Bailey (1989).

Ages, determined by the potassium-argon method, are well known for most of the flows described herein and range from about 155 to 64 ka. Ages for map numbers 22, 46, and 23 (Table 1 in Mankinen and others, 1986) in the south moat of the caldera remain unconfirmed. Because within flow contents of K_2O are in good agreement but argon contents are not, and because large variations in $^{40}Ar_{rad}$ exist, the three flows probably contain extraneous argon (Mankinen and others, 1986). The flow at locality 22 is overlain by the Casa Diablo till of Curry (1971) which may be either Mono Basin or Tahoe in age (Bailey, 1989). This entire sequence of lava flows is capped by moraines of the Tioga glaciation (Bailey, 1989). Ages determined for the Tioga glaciation using the ^{36}Cl method (Phillips and others, 1990) range from 23.1 to 20.4 ka, and Bursik and Gillespie (1993) consider 25.2 ka to be a

maximum age for this glaciation. The Tahoe glaciation is younger than 119 ± 7 ka (Gillespie and others, 1984) and has been dated as occurring between 65.8 and 55.9 ka by the ^{36}Cl method (Phillips and others, 1990). Phillips and others (1990) consider the most likely ages for the Mono Basin tills to be between 120 and 110 ka based on the ^{36}Cl method. However, Bursik and Gillespie (1993) are skeptical of ^{36}Cl dates in this age range. At the present time, ages for this sequence remain poorly constrained and the ages for the flows at localities 22 (129 ± 26 ka) and 23 (64 ± 14 ka) are tentatively considered maximum ages. The flow at locality 49 has not been dated directly but its stratigraphic position between flows at sites 28 and 39 constrains its age to be 99 ± 16 ka.

METHODS

Sample Selection Criteria

Specimens used in the paleointensity experiments were chosen primarily on the basis of their behavior during strong field thermomagnetic analysis. These analyses were made in a nitrogen atmosphere to inhibit oxidation using an automatic recording balance (Doell and Cox, 1967). Specimens were heated and cooled at a rate of 10°C/min in applied fields between 200 and 450 mT. Curie temperatures (T_c's) were measured using the method of Grommé and others (1969). Curie temperatures ranging from about 505° to 575°C (Table 1 and Fig. 1), and induced magnetization (J_s) acquisition curves nearing saturation at about 300 mT (Fig. 2) indicate that the carrier of remanence in these rocks is a low-Ti titanomagnetite. Thermomagnetic curve types given correspond to those described in Mankinen and others (1985). Samples exhibiting type 2a curves were preferred for paleointensity determination because previous studies (e.g., Prévot and others, 1985) have shown that such rocks are the best candidates for providing reliable paleointensity estimates.

Secondary criteria used included the rock magnetic properties given in Table 1, and a requirement that the specimen selected should have a remanence direction close to the mean direction for the flow in order to avoid samples that contain spurious components of magnetization. Saturation magnetization and saturation remanence (J_{rs}), in most cases, were determined for the same samples later used in the strong-field thermomagnetic measurements. J_{rs} was measured after magnetizing the samples in 900 mT, and J_s was determined by plotting the variation of the induced magnetization (in fields ranging from 0 to 900 mT) against the reciprocal of the applied field and extrapolating to $H = \infty$. Many samples had J_{rs}/J_s values near 0.1 (Table 1) which is indicative of multidomain to pseudo-single-domain titanomagnetite grains. Whenever possible, samples with values greater than about 0.17 were used in the paleointensity experiments because Dunlop (1983) has shown that basalts with a range of values between 0.17 and 0.27 display single-domain behavior, and such samples are preferred for paleointensity experiments (Levi, 1977).

Weak-field susceptibilities were measured at 800 Hz using a commercial bridge at room temperature, and the in situ Koenigsberger ratio, Q_n, was calculated using the present day field intensity at Long Valley (52.5 μT). Because susceptibility is dependent on both grain size of the magnetic minerals and their concentration, the highest values of Q_n within a flow usually indicate the smallest grain sizes.

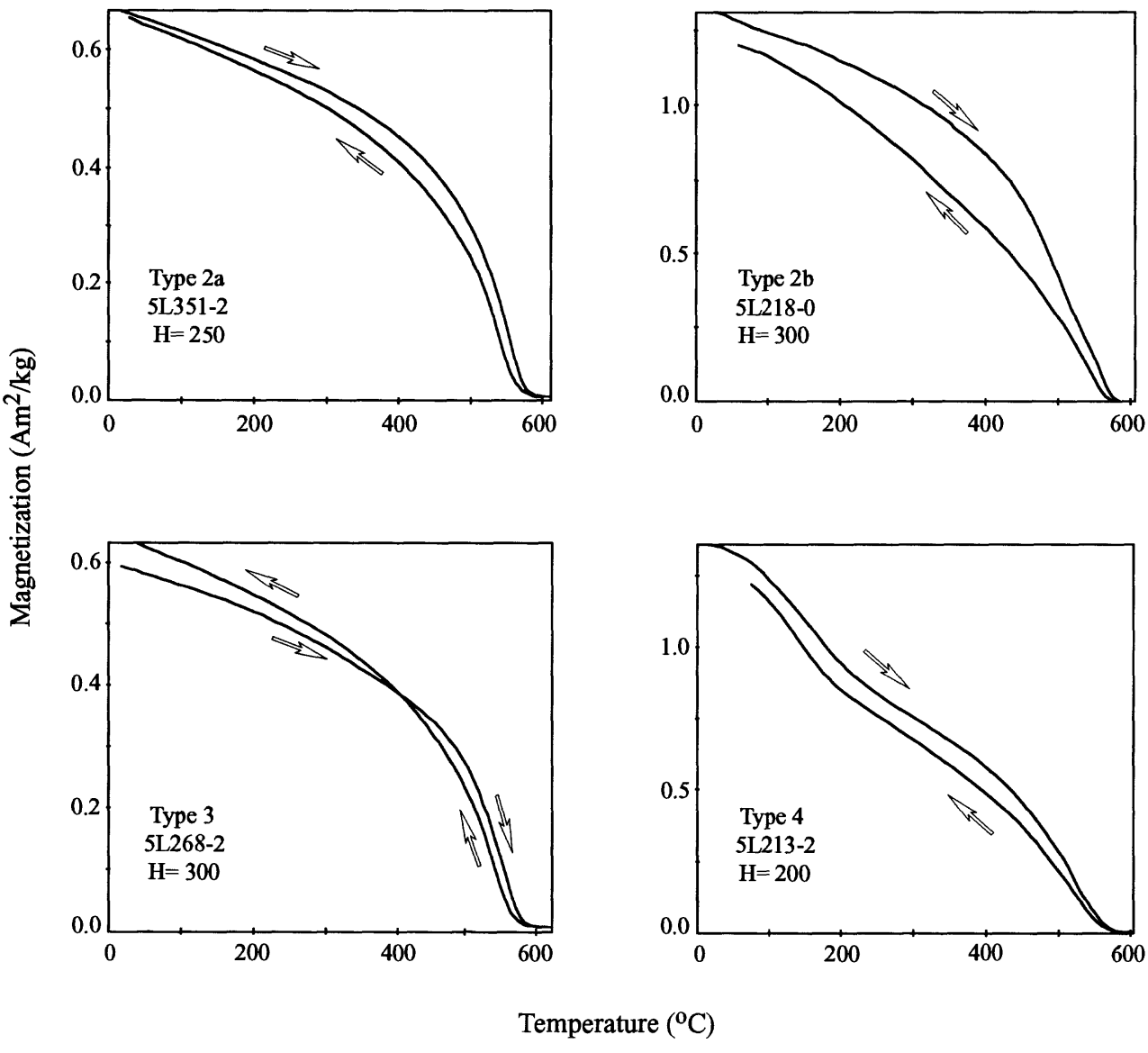

Figure 1. Selected strong-field thermomagnetic curves for samples from Long Valley caldera. Experiments were run in a nitrogen atmosphere at heating and cooling rates of 10°C/min. Heating and cooling curves indicated by arrows. H is applied field in mT. Curve types described in Mankinen and others (1985).

TABLE 1. MAGNETIC PROPERTIES OF SAMPLES FROM VOLCANIC ROCKS OF LONG VALLEY CALDERA

Flow No.	Sample	J_{rs}	J_s	J_{rs}/J_s	J_{nrm}	X	Q_n	T_c
	5L210-2	0.240	1.81	0.133	2.89	23.4	3.0	545
23	5L211-1	-----	2.02	-----	3.70	33.6	2.6	537
	5L212-2	0.306	1.69	0.181	2.33	16.3	3.4	564
	5L213-2	0.343	1.71	0.201	3.38	17.6	4.6	214, 559
	2C564-0	-----	-----	-----	----	----	----	545
	5L234-2	0.296	2.02	0.147	1.86	19.9	2.2	554
	5L235-2	0.530	2.53	0.209	2.69	23.8	2.7	565
53	5L236-1	-----	2.20	-----	1.68	22.6	1.8	564
	5L237-2	0.374	2.01	0.186	1.41	15.8	2.1	574
	5L238-2	0.344	2.07	0.166	1.08	19.1	1.4	564
	5L239-2	0.361	2.02	0.179	1.54	18.7	2.0	570
	5L353-1	-----	0.938	-----	0.82	15.5	1.2	510
	5L354-2	0.0836	0.91	0.092	----	----	----	543
31	5L355-0	0.199	1.27	0.157	8.67	15.3	13.5	551
	5L356-2	0.0591	0.962	0.061	----	----	----	510
	5L358-2	0.051	0.843	0.061	----	----	----	505
	5L359-0	0.0769	0.873	0.088	1.47	12.0	2.9	548
	5L344-0	0.173	0.854	0.203	6.56	8.78	17.9	571
	5L345-1*	-----	0.955	-----	4.11	11.4	8.6	565
	5L346-2	0.112	0.556	0.201	3.95	6.42	14.7	575
28	5L347-2	0.196	0.946	0.207	3.19	8.17	9.4	573
	5L348-2	0.142	0.913	0.156	4.90	9.16	12.8	571
	5L349-2	0.125	0.791	0.158	----	----	----	516
	5L351-2	0.195	0.976	0.200	3.68	8.53	10.3	575
	5L444-1	0.114	1.56	0.073	2.75	23.6	2.8	525
	5L445-1	0.211	1.54	0.137	2.93	15.7	4.5	565
	5L446-1	0.219	1.58	0.139	3.07	15.0	4.9	564
49	5L447-1	-----	1.65	-----	2.69	21.7	3.0	532
	5L448-1	0.176	1.42	0.124	4.05	18.7	5.2	556
	5L449-1	0.228	1.51	0.151	7.92	19.4	9.8	556
	5L450-1	0.186	1.47	0.127	5.88	18.5	7.6	539
	5L451-1	0.209	1.55	0.135	2.99	16.6	4.3	566
	5L334-2	0.0833	0.599	0.139	----	----	----	278, 523
39	5L335-1	-----	0.717	-----	1.30	11.6	2.7	276, 503
	5L337-0	0.0954	0.740	0.129	----	----	----	280, 505
	5L340-0	0.0453	0.198	0.229	3.14	2.45	3.1	541
	5L385-1	0.315	0.997	0.316	10.7	7.87	32.5	170, 578
	5L386-1	0.227	0.914	0.248	5.52	7.60	17.4	580
	5L387-1	0.330	1.14	0.290	3.55	8.97	9.5	577
20	5L388-2	0.325	1.40	0.232	10.8	12.7	20.4	577
	5L389-1	0.171	0.914	0.187	3.55	7.70	11.0	579
	5L390-1	0.106	0.758	0.140	2.72	6.70	9.7	576
	5L391-1	0.121	0.850	0.142	3.08	8.07	9.1	573
	5L392-1*	-----	0.960	-----	3.49	8.14	10.3	570

TABLE 1. (continued)

	5L217-2	0.258	1.24	0.208	4.72	12.8	8.8	219, 576
	5L218-0	0.243	1.63	0.149	4.65	16.3	6.8	575
	5L219-1	-----	1.44	-----	4.41	19.5	5.4	558
22	5L220-2	0.202	1.38	0.146	4.05	15.1	6.4	572
	5L221-2	0.247	1.34	0.184	6.52	14.3	10.9	246, 576
	5L223-2	0.193	0.912	0.212	3.89	8.00	11.7	574
	5L224-2	0.215	1.46	0.147	3.67	15.3	5.5	572
	2C502-0	-----	-----	-----	----	----	----	560
	5L258-2	0.0770	0.544	0.142	1.98	5.53	8.6	570
	5L259-0	0.154	0.880	0.175	2.04	7.40	6.6	575
	5L261-1	-----	0.862	-----	2.41	9.45	6.1	577
15	5L262-2	0.109	0.710	0.154	2.86	5.25	13.0	572
	5L263-2	0.164	0.792	0.207	1.99	5.20	9.2	577
	5L264-2	0.243	0.869	0.280	2.20	6.03	8.7	582
	5L265-2	0.286	1.02	0.280	4.60	8.28	13.3	576
	5L267-2	0.0951	0.657	0.145	2.43	5.74	10.1	568
	5L268-2	0.125	0.816	0.153	1.95	6.02	7.8	571
	5L269-2	0.145	1.01	0.144	2.99	9.41	7.6	569
16	5L270-1	0.226	0.996	0.227	3.18	7.18	10.6	574
	5L271-1	----	1.13	-----	3.04	8.77	8.3	568
	5L272-2	0.204	0.907	0.225	2.71	6.96	9.3	573
	5L273-2	0.134	0.862	0.155	1.83	7.00	6.3	561

Note: Flow number corresponds to map number in Mankinen and others (1986); J_{rs} is saturation remanence (Am^2/kg); J_s is saturation magnetization (Am^2/kg); J_{nrm} is intensity of natural remanent magnetization (A/m); X is volume susceptibility ($x10^{-3}$); Q_n is in situ Koenigsberger ratio (J_{nrm}/XF, where F= 52.5 μT); T_c is Curie temperature (°C).

* denotes rock magnetic properties and Thellier experiments performed on adjacent specimens.

Paleointensity Experiments

The paleointensity experiments were performed in a nitrogen atmosphere using the apparatus described by Prévot and others (1985). The average ambient field within the furnace array was about 70 nT. The paleointensity method used was that developed by Thellier and Thellier (1959) as modified by Coe (1967). At every temperature, the specimens were first heated and cooled in a "zero" field (the ambient field), and the remaining natural remanent magnetization (NRM) was measured at room temperature using a cryogenic magnetometer. A field of 50 μT, which is close to the present field intensity at Long Valley, was applied parallel to the cylindrical axes of the specimens during the second of each pair of heating steps. This field was applied throughout the entire, several-hours-long heating and cooling cycle (Levi, 1975).

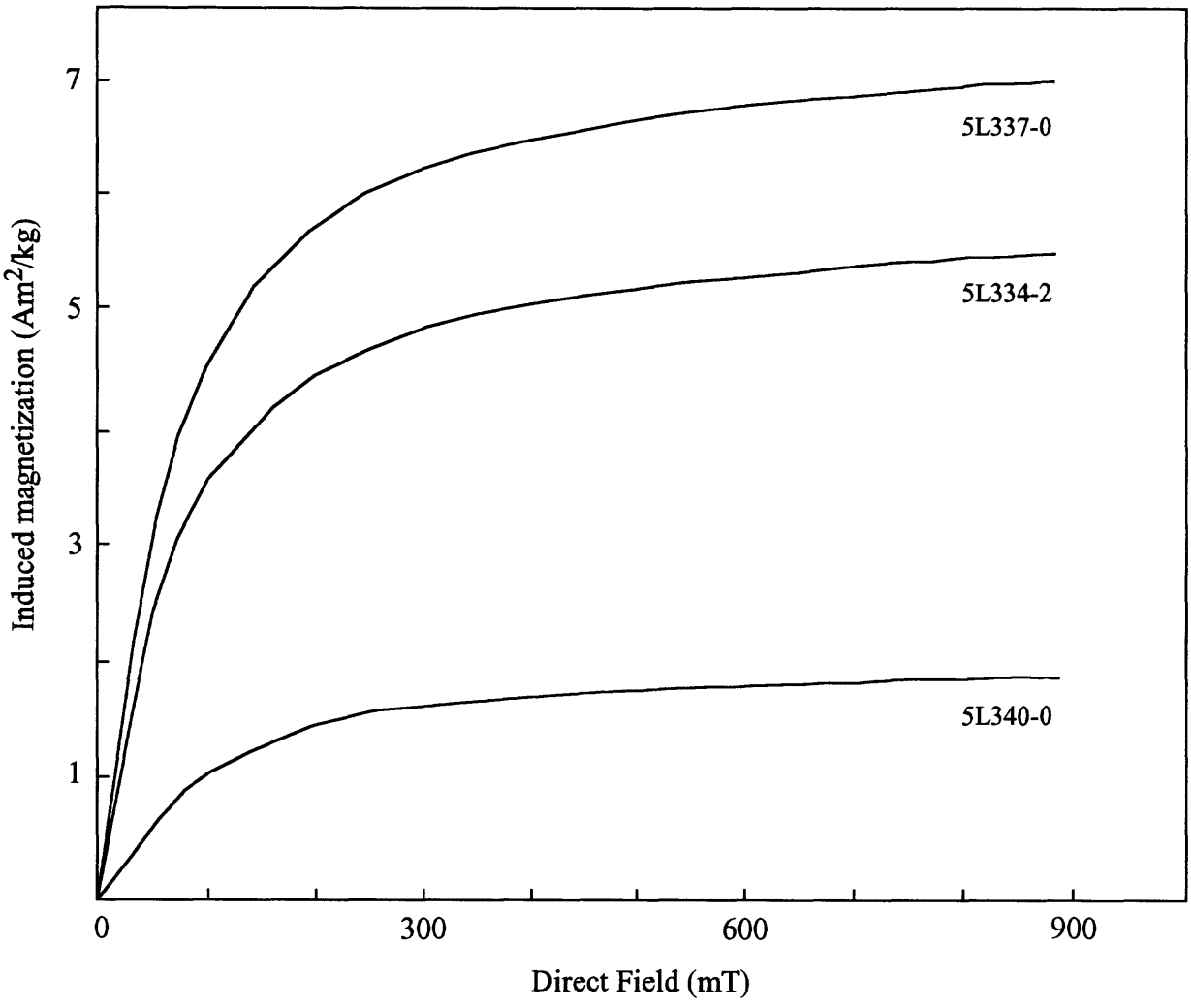

Figure 2. Acquisition of induced magnetization for samples from site #39.

Magnetic stability during the heating experiments was tested by redetermining the partial thermoremanent magnetization (PTRM) at a given low-temperature interval after the samples had been heated to successively higher temperatures (using the sliding PTRM-check method described by Prévot and others (1985)). The method of Coe and others (1984) was used to test whether appreciable amounts of chemical remanent magnetization (CRM) were acquired during the laboratory heatings. Weak-field susceptibility was measured after each heating step to help detect mineralogical changes that could affect the reliability of the results.

Data Analysis

Paleointensity data are best displayed on a NRM-TRM diagram (Nagata and others, 1963), typical examples of which are shown in Figure 3. The NRM in these diagrams is the component directed along the stable NRM direction remaining after heating to a temperature, T_i. The TRM plotted is the component projected onto the applied field direction that was acquired in the interval between T_i and room temperature. For an ideal sample, all such NRM/TRM points will fall on a straight line with the negative slope equal to the ratio of the ancient Earth's field to the applied laboratory field. In practice, however, most samples will begin to chemically alter at some point during the heating experiments and only a fraction of the total NRM will yield reliable paleointensity values.

Several factors were used to evaluate the experimental data before a determination of the paleointensity was made. (1) No paleointensity was estimated unless at least four NRM-TRM points within a given range of unblocking temperatures fell on a straight line and spanned a range of 15% or more of the total NRM intensity. Because a recently acquired viscous remanent magnetization (VRM) could have a direction quite close to that of the original TRM and therefore be difficult to detect, the initial room temperature measurement was not used in any estimate. (2) PTRM checks needed to closely approximate the values previously determined for the same temperatures. Any systematic deviation of these checks from the least squares line was taken as an indication that the TRM spectrum had been altered. (3) No appreciable amounts of CRM should be detectable within the linear segment analyzed using the method of Coe and others (1984). (4) Sudden deviations in the rate of change in weak-field susceptibility could also be an indication of magnetochemical changes.

RESULTS

Paleointensity estimates and associated statistical parameters are given in Table 2. Because significant differences in the measures of quality are commonly observed for samples within a single unit, both unweighted and weighted mean paleointensities were determined and the virtual dipole moment (VDM) was calculated from the weighted mean. Weighted means were calculated using the weighting factor defined by Prévot and others (1985), and these are shown in Figure 4. Because the weighting factor used differs from the weight derived from the theory of errors and cannot, therefore, be used to calculate a weighted standard error, uncertainties in the paleointensity estimate are expressed by using the standard deviation about the unweighted mean. Substantial differences in apparent paleointensity can occur in a single lava flow and, for that reason, paleointensity values listed in Table 2 that are based on fewer than three determinations should be considered tentative.

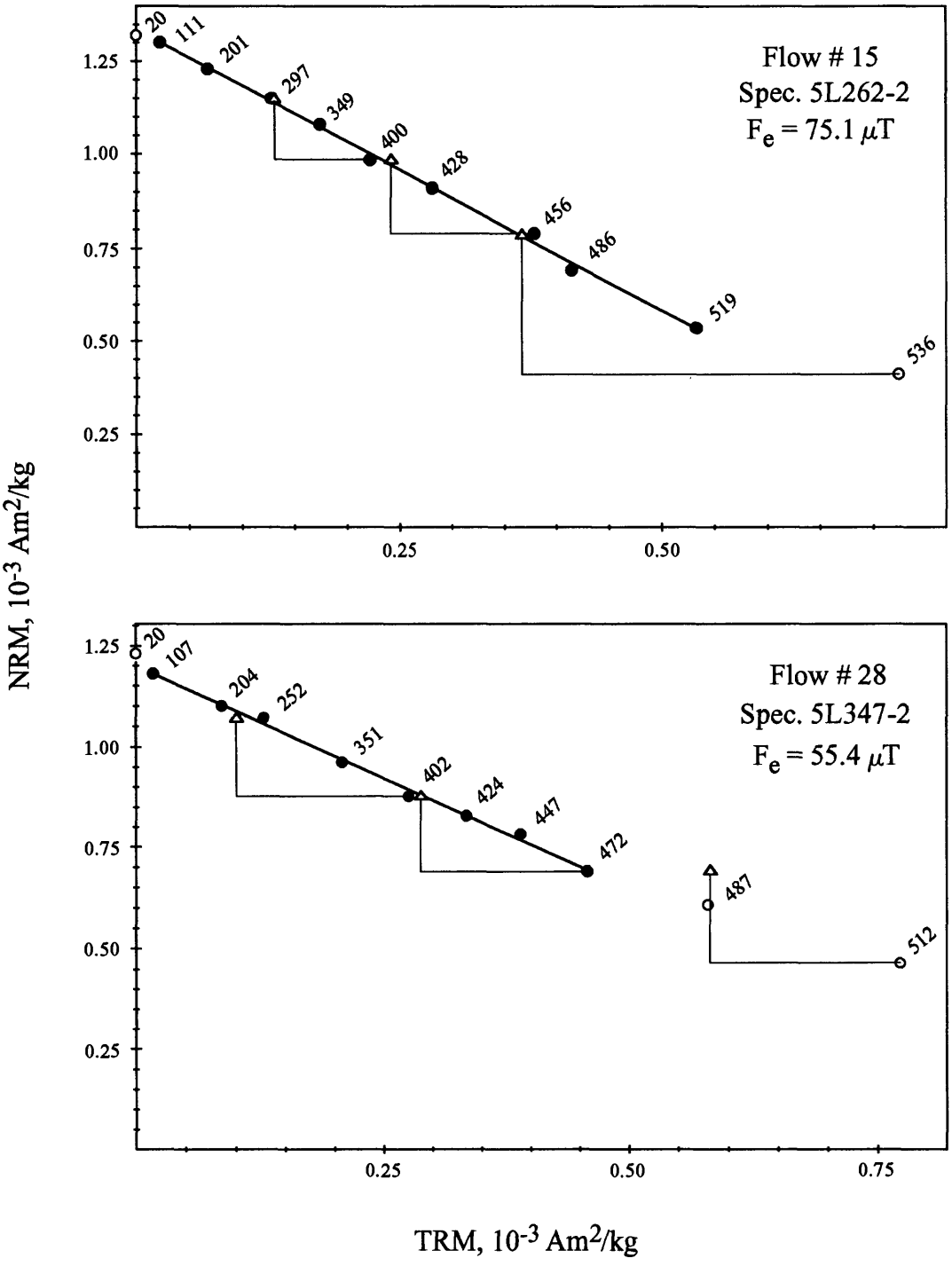

Figure 3. Typical examples of paleointensity data for the Long Valley lava flows. Circles are NRM-TRM points calculated for each double heating at the temperature indicated near each point. Lines connect each PTRM check (triangles) to the NRM-TRM point corresponding to the maximum temperature to which the specimen was heated before performing the check. Solid circles are NRM-TRM points used to determine the least-squares line, shown as the heavy, solid line in the figures; open circles are points not used in the calculations.

TABLE 2. PALEOINTENSITY DETERMINATIONS FOR LAVA FLOWS FROM LONG VALLEY CALDERA

Flow No.	Age (ka)	Samp. No.	N	T_{mn} (°C)	T_{mx} (°C)	f	g	q	$F_e \pm \sigma(F_e)$ (μT)	$\overline{F}_e \pm$ s.d. (μT)	$\langle F_e \rangle$ (μT)	VDM (VADM) (10^{22} Am^2)
23	064	5L212-1*										
53	064	5L237-2	4	107	248	0.123	0.651	1.0	20.6 ± 1.7			4.51
31	086	5L355-0*										
		5L344-0	7	106	445	0.134	0.691	2.1	47.2 ± 2.1			
		5L345-2	9	106	483	0.289	0.813	10.9	46.9 ± 1.0			
28	095	5L347-2	8	107	471	0.408	0.846	13.8	55.4 ± 1.4	48.6 ± 5.3	49.7	9.79
		5L348-2	9	106	485	0.372	0.837	8.6	41.4 ± 1.5			
		5L351-2	9	105	480	0.438	0.863	9.5	51.9 ± 2.0			
		5L444-1	4	104	344	0.216	0.593	4.8	56.1 ± 1.5			
49	099	5L446-1	4	104	346	0.191	0.620	1.5	54.3 ± 4.4	53.8 ± 2.5	54.4	9.75
		5L449-1	7	107	476	0.214	0.804	3.7	51.1 ± 2.4			
		5L450-1*										
39	103	5L340-0	7	201	495	0.225	0.792	4.6	28.5 ± 1.1			5.23
		5L386-1	6	199	464	0.283	0.760	3.2	56.8 ± 3.8			
		5L387-1	9	104	504	0.479	0.858	18.8	48.4 ± 1.1			
20	108	5L388-2	9	198	553	0.504	0.777	15.7	40.6 ± 1.0	49.1 ± 5.8	47.4	8.62
		5L389-1	7	107	485	0.439	0.815	8.7	50.6 ± 2.1			
		5L392-2	7	107	484	0.426	0.798	6.9	49.0 ± 2.4			
22	129	5L220-2*										
		5L223-2	9	110	519	0.348	0.845	8.5	45.5 ± 1.6			8.03
		5L258-2	6	348	519	0.357	0.789	5.3	50.2 ± 2.7			
15	154	5L262-2	9	110	519	0.574	0.860	25.3	75.1 ± 1.5	53.4 ±14.8	60.1	8.02
		5L263-2	6	201	458	0.427	0.789	7.7	46.1 ± 2.0			(10.7)
		5L265-2	6	99	422	0.250	0.766	7.0	42.3 ± 1.2			
		5L267-2	6	398	528	0.354	0.782	6.7	42.3 ± 1.8			
16	155	5L268-2	6	99	425	0.360	0.785	5.8	76.8 ± 3.8	59.4 ±17.3	58.6	7.69
		5L269-2*										(10.4)
		5L270-1	7	99	458	0.496	0.809	11.5	59.0 ± 2.1			

Note: Flow number corresponds to map number in Mankinen and others (1986); N is the number of points in the T_{mn}-T_{mx} interval; T_{mn} and T_{mx} are the minimum and maximum of the temperature range used to determine paleointensity; f, g, and q are the NRM fraction, gap factor, and quality factor, respectively [Coe et al., 1978]; F_e is the paleointensity estimate for an individual specimen, and $\sigma(F_e)$ is its standard deviation [Prévot et al., 1985]; $\overline{F}_e$ is the unweighted average paleointensity, with the plus and minus corresponding to the standard deviation; $\langle F_e \rangle$ is the weighted average paleointensity using the weighting factor, fg/s, of Prévot et al. [1985]; VDM is the virtual dipole moment [Smith, 1967]; VADM is the virtual axial dipole moment [Barton et al., 1979].

* denotes those specimens for which a paleointensity could not be determined.

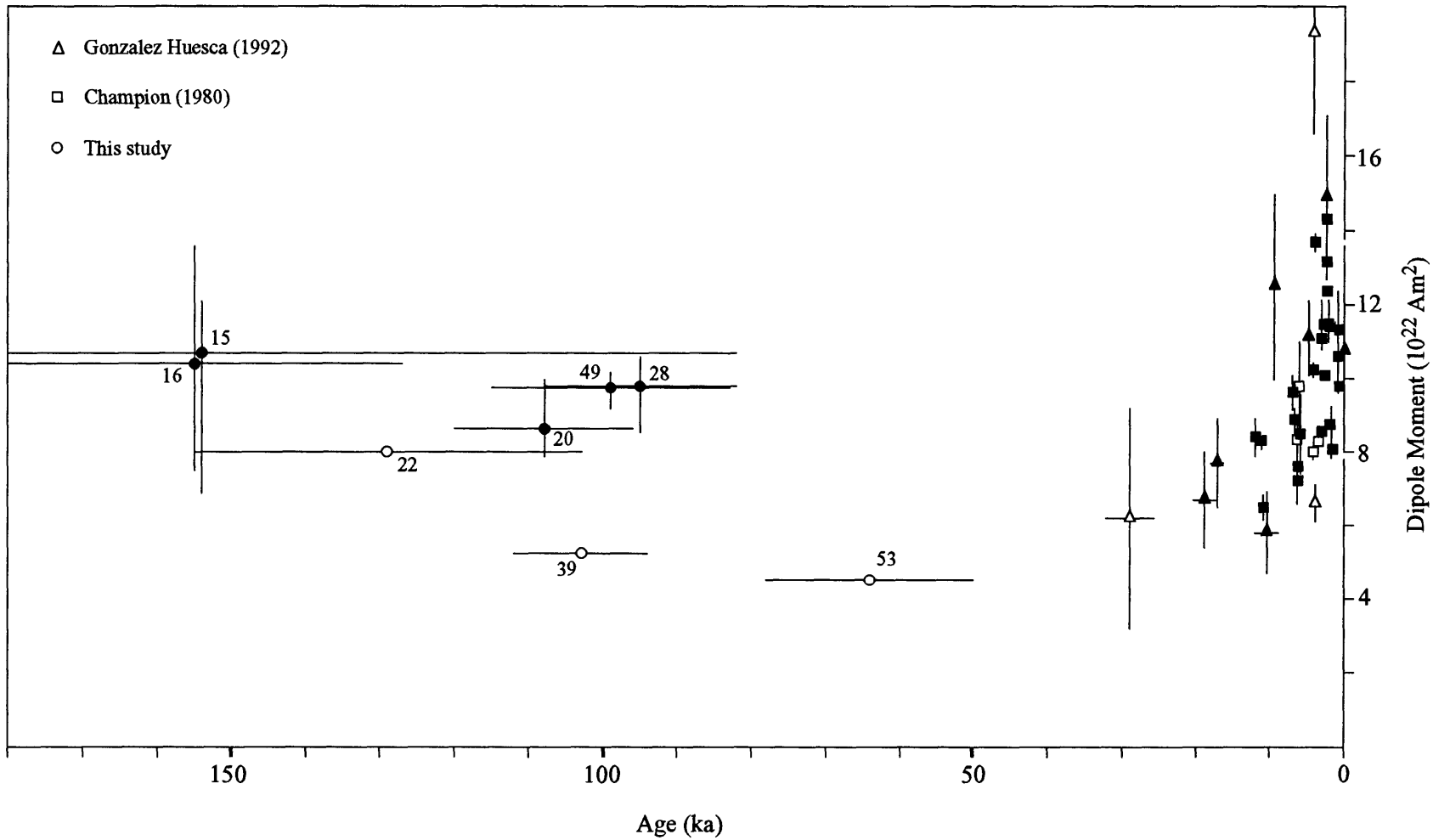

Figure 4. Paleointensity as a function of age for lava flows from southwestern North America. Labels are flow designations from Table 2. Data from Champion (1980) and Gonzalez Huesca (1992) are from lava flows dated by the ^{14}C method. These ages have not been corrected for isotopic fractionation or secular changes in atmospheric ^{14}C. Open symbols are values based on fewer than three determinations.

Specimens from localities 16 (5L269-2), 22 (5L220-2), and 23 (5L212-1) yielded NRM-TRM diagrams with excessive systematic curvature and were considered unsuitable for determining a paleofield (see factor #1 above). The curvature exhibited by these specimens is typical of samples containing multidomain magnetite (Levi, 1977). Magnetochemical changes occurred below 300°C in specimens from localities 31 (5L355-0) and 49 (5L450-1) as evidenced by failure of PTRM checks (site #31) and radical changes in weak-field susceptibility (site #49).

The data from the single sample analyzed from the 64 ka unit was unsuitable for determining a paleointensity. The same unit was sampled also at locality 53 (Bailey, 1974; Mankinen and others, 1986) and a sample from this site indicates a weak paleofield of 20.6 μT. However, the quality factor for this determination is low and additional samples need to be measured in order to confirm this result. Localities 15 and 16 are in a structural block that may have been tilted (Mankinen and others, 1986) and a virtual axial dipole moment (VADM) has been calculated for both units using the magnetic field direction that would be produced at Long Valley by an axially symmetric dipole field. Both the VADM and VDM (which uses the measured remanence direction) are given in Table 2, and the VADM's are plotted in Figure 4.

DISCUSSION

Data from this study are shown in Figure 4 which also includes other available paleointensity determinations from southwestern North America. Champion (1980) used the Thelliers' method to obtain paleointensity estimates for 28 radiocarbon-dated lava flows from the western United States. A detailed record of paleointensity variations in the southwestern United States for the past 2000 years was determined by Sternberg (1989) using the Thelliers' method on archeological artifacts of the Hohokam, Anasazi, and Mogollon cultures. This record is not shown here because of the difficulty of accurately representing these data at the scale of Figure 4. The agreement in this time range is quite good, however, among the data from Champion (1980), Sternberg (1989), and from unpublished thesis as summarized by Sternberg.

Data from Mexico were reported by Gonzalez Huesca (1992) who calculated paleointensities on ^{14}C-dated lava flows generally based on results obtained using both the Thelliers' method and that developed by Shaw (1974). Only the paleointensities on the 29 and 3.8 ka flows were based on the Shaw method alone. Peaks in paleointensity determined by Gonzalez Huesca (1992) at about 2.4 and 4.1 ka are in agreement with the results of Champion (1980) although the value at 4.1 ka determined by Gonzalez Huesca seems abnormally high. Another high value that she obtained for a flow at 9.4 ka (Fig. 4) corresponds well with a world-wide peak at about that time as shown in Figure 5.

Figure 5 summarizes current knowledge about the late Quaternary field as deduced from paleointensity studies on volcanic rocks and archaeological artifacts world-wide. The 50-0 ka interval is adapted from Mankinen and Champion (1993*b*) and shows the VDM curve from Hawaii (solid curve) and the world-wide mean curve for Holocene time (stippled pattern) from the compilation of McElhinny and Senanayake (1982). The dashed horizontal line is the world-wide average VDM for Holocene time (McElhinny and Senanayake, 1982); this VDM (8.75×10^{22} Am^2) differs only slightly from the mean VDM for Quaternary time (8.68×10^{22} Am^2) calculated by Otake and others (1993). Data points summarized in Mankinen and Champion (1993*b*) are shown as crosses, with symbols representing data not available at the time that report was prepared. Data shown are VDM's except

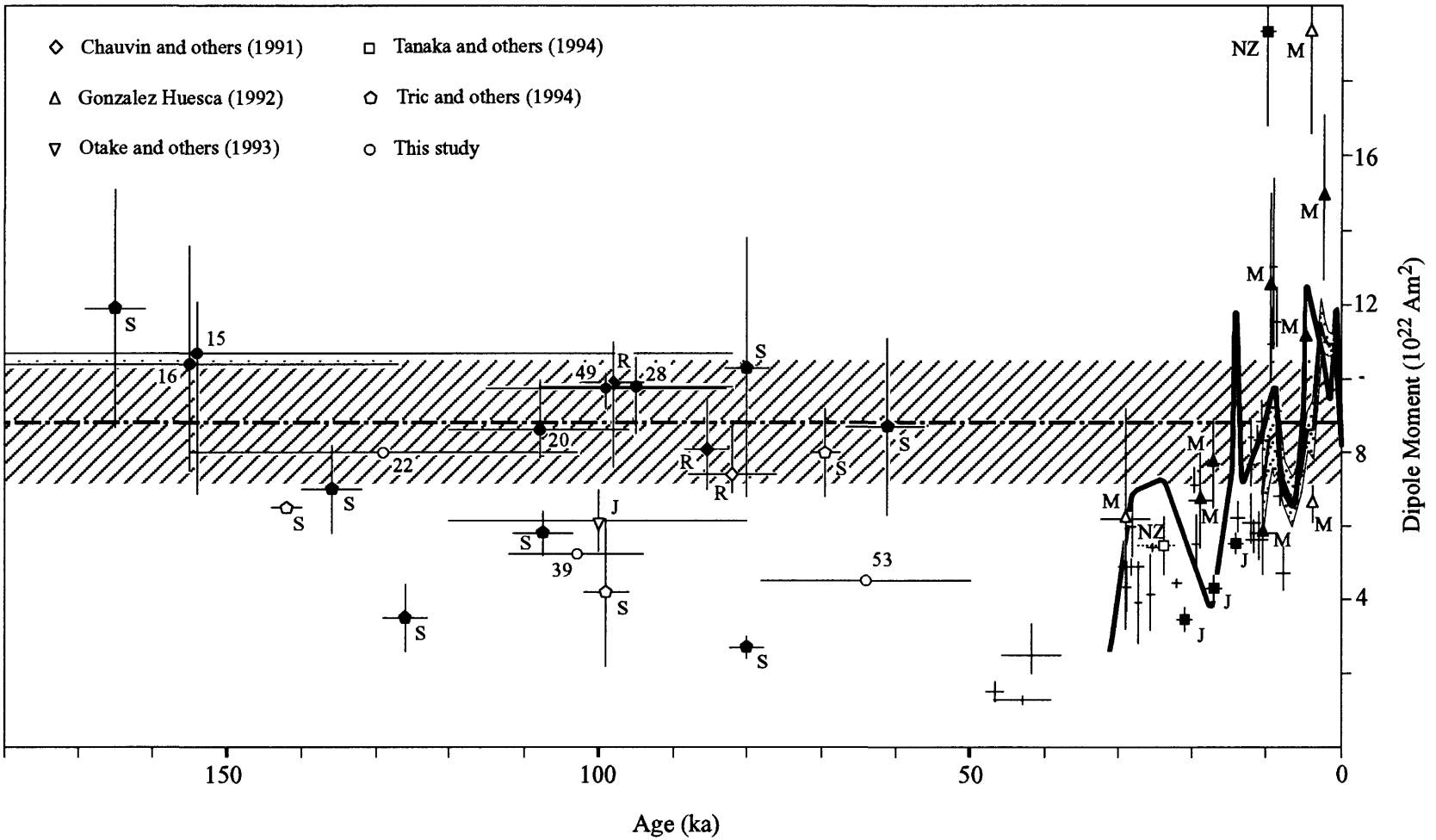

Figure 5. Paleointensity data from this study compared with available data world-wide. Interval between 50 and 0 ka modified from Mankinen and Champion (1993) with crosses representing data summarized therein. Labeled symbols correspond to data not available when that report was prepared. Solid curve is VDM curve from Hawaii (Mankinen and Champion, 1993*a*,*b*) and dotted pattern is the 95% confidence envelope about the world-wide mean curve for Holocene time (McElhinny and Senanayake, 1982) based on the archeomagnetic record. Dashed horizontal line is the world-wide average dipole moment for Holocene time (McElhinny and Senanayake, 1982) and its standard deviation (ruled area). Numbered data are from Table 2, and others are from Japan (J), Mexico (M), New Zealand (NZ), Reunion Island (R), and Mount Etna, Sicily (S).

where unavailable. Data from Champion (1980) are not shown on this figure because they have been included in the calculation of the mean Holocene curve (McElhinny and Senanayake, 1982).

As mentioned above, the high value for 9.4 ka reported by Gonzalez Huesca (1992) corresponds well with other high values at about this time (Fig. 5). A very high paleointensity has been obtained from a 10 ka rhyolite lava flow from New Zealand (Tanaka and others, 1994) that also may be related to the high dipole field at about 9 ka but enhanced by the nondipole field. The interval of lower than normal paleointensities immediately preceding Holocene time that was first noted by McElhinny and Senanayake (1982) continues to be borne out with the addition of new data (Fig. 5). The only exception seems to be the high paleointensity from a single Hawaiian lava flow erupted at 14 ka, and Mankinen and Champion (1993) interpreted this result to be due to the nondipole field. Although data are scarce in the 90 to 50 ka interval, the single determination from the flow at site 53 (64 ka, Table 2) is suggestive that the interval of abnormally low paleointensities may have been quite prolonged. However, a flow of approximately the same age from Mount Etna (Sicily) yields a paleointensity that is within the normal range (Tric and others, 1994). Data from Réunion Island (Chauvin and others, 1991) and Mount Etna (Tric and others, 1994) indicate that the intensity of the field had been in the normal range until about 80 ka (Fig. 5). Note that there are two lava flows dated at 80 ka from Mount Etna and that one yields an anomalously low paleointensity. There may have been another, shorter interval of low paleointensity slightly before 100 ka as indicated by lavas at site 39 (Table 2), in Japan (Otake and others, 1993), and on Mount Etna (Tric and others, 1994).

Absolute values of paleointensity such as those determined by the Thelliers' (1959) method can only be obtained from rocks and archeological artifacts that have acquired a thermoremanent magnetization upon cooling in the Earth's magnetic field. However, each determination represents an "instantaneous" reading of geomagnetic field intensity and determinations can be unevenly distributed over time. In order to overcome this problem of irregularly spaced determinations, attempts have been made to obtain continuous, relative paleointensity records from sedimentary sequences. Although relative paleointensity determinations remain controversial, when the sedimentary sequences are carefully selected their records often show broad similarities to known world-wide records.

Relative paleointensity records covering the period of time shown in Figure 5 have been obtained from three marine cores from the western Indian Ocean by Meynadier and others (1992). They combined their data with those obtained previously from marine cores in the Mediterranean Sea (Tric and others, 1992) to produce a synthetic record for the region. A sketch of Meynadier and others' (1992) synthetic curve was superimposed on the data from Figure 5 and is shown in Figure 6. Considerable similarities exist between the relative and absolute paleointensity records for the interval between about 40 and 9 ka. The tentative result from the 64 ka lava flow (site #53) also is consistent with the synthetic record, but results from two Mount Etna lava flows erupted between 70 and 60 ka are not. Values from the older lava flows in Long Valley and those on Réunion Island, in general, do not agree with the relative paleointensities. Several of the older Mount Etna lava flows, on the other hand, are in excellent agreement with this record. These examples emphasize the necessity of averaging data from many globally distributed localities before a true picture of the dipole field can be obtained. The same is true for relative paleointensity records.

ACKNOWLEDGMENTS

I thank Lisa Paulick for assistance with the Thellier experiments.

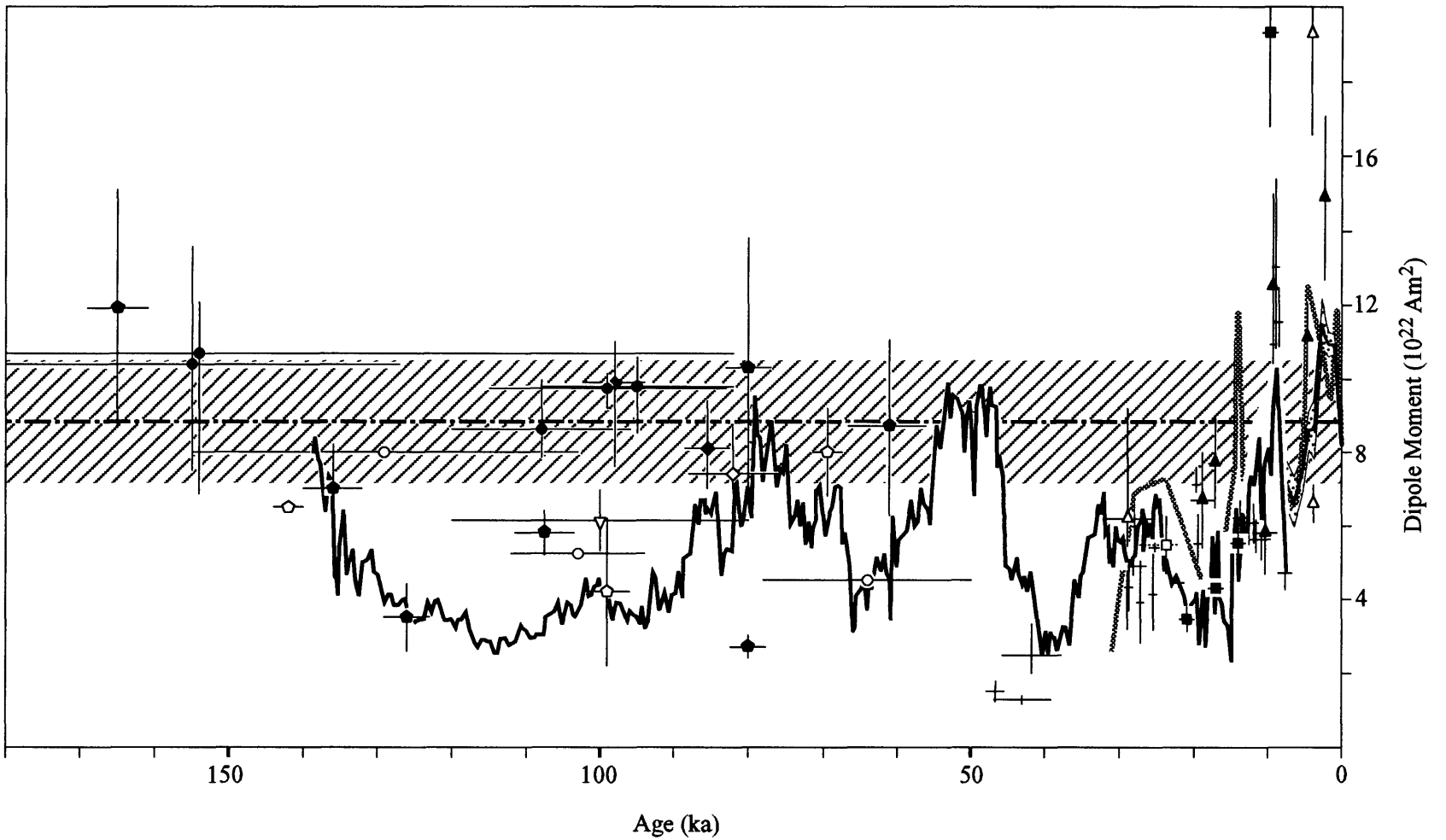

Figure 6. Data from Figure 5 compared with a synthetic record (heavy, solid curve) obtained by stacking relative paleointensity records of marine sedimentary cores from the Mediterranean Sea and the western Indian Ocean (Meynadier and others, 1992).

REFERENCES

Bailey, R.A., 1974, Preliminary geologic map and cross sections of the Casa Diablo geothermal area, Long Valley caldera, Mono County, California: U.S. Geological Survey Open-File Map OF 74-1007, 2 sheets, scale 1:20,000.

Bailey, R.A., 1989, Geologic map of the Long Valley caldera, Mono-Inyo Craters volcanic chain, and vicinity, eastern California: U.S. Geological Survey Miscellaneous Investigations Map I-1933, 2 sheets, scale 1:62,500.

Bailey, R.A., Dalrymple, G.B., and Lanphere, M.A., 1976, Volcanism, structure, and geochronology of Long Valley caldera, Mono County, California: Journal of Geophysical Research, v. 81, p. 725-744.

Bard, E., Hamelin, B., Fairbanks, R.G., and Zindler, A., 1990, Calibration of the ^{14}C timescale over the past 30,000 years using mass spectrometric U-Th ages from Barbados corals: Nature, v. 345, p. 405-410.

Barton, C.E., Merrill, R.T., and Barbetti, M., 1979, Intensity of the Earth's magnetic field over the last 10 000 years: Physics of the Earth and Planetary Interiors, v. 20, p. 96-110.

Bursik, M.I., and Gillespie, A.R., 1993, Late Pleistocene glaciation of Mono Basin, California: Quaternary Research, v. 39, p. 24-35.

Champion, D.E., 1980, Holocene geomagnetic secular variation in the western United States -- Implications for the global geomagnetic field: U.S. Geological Survey Open-File Report 80-824, 326 p.

Chauvin, A., Gillot, P.-Y., and Bonhommet, N., 1991, Paleointensity of the Earth's magnetic field recorded by two late Quaternary volcanic sequences at the Island of Réunion (Indian Ocean): Journal of Geophysical Research, v. 96, p. 1981-2006.

Coe, R.S., 1967, The determination of paleo-intensities of the Earth's magnetic field with emphasis on mechanisms which could cause non-ideal behavior in Thellier's method: Journal of Geomagnetism and Geoelectricity, v. 19, p. 157-179.

Coe, R.S., Grommé, S., and Mankinen, E.A., 1978, Geomagnetic paleointensities from radiocarbon-dated lava flows on Hawaii and the question of the Pacific nondipole low: Journal of Geophysical Research, v. 83, p. 1740-1756.

Coe, R.S., Grommé, S., and Mankinen, E.A., 1984, Geomagnetic paleointensities from excursion sequences in lavas on Oahu, Hawaii: Journal of Geophysical Research, v. 89, p. 1059-1069.

Curry, R.R., 1971, Glacial and Pleistocene history of the Mammoth Lakes Sierra, California -- A geologic guidebook: University of Montana Geological Series Publication, no. 2, p. 1-49.

Doell, R.R., and Cox, A., 1967, Recording magnetic balance, in Collinson, D.W., Creer, K.M., and Runcorn, S.K., eds., Methods in palaeomagnetism: Amsterdam, Elsevier, p. 440-441.

Dunlop, D.J., 1983, Determination of domain structure in igneous rocks by alternating field and other methods: Earth and Planetary Science Letters, v. 63, p. 353-367.

Gillespie, A.R., Huneke, J.C., and Wasserburg, G.J., 1984, Eruption age of a $\approx$100,000-year-old basalt from ^{40}Ar-^{39}Ar analysis of partially degassed xenoliths: Journal of Geophysical Research, v. 89, p. 1033-1048.

Gonzalez Huesca, I.S., 1992, La variacion secular en Mexico central durante los ultimos 30,000 años por medio del estudio magnetico de lavas [PhD thesis]: Mexico D.F., Universidad Nacional Autonoma de Mexico, 147 p.

Grommé, C.S., Wright, T.L., and Peck, D.C., 1969, Magnetic properties and oxidation of iron-titanium oxide minerals in Alae and Makaopuhi lava lakes, Hawaii: Journal of Geophysical Research, v. 74, p. 5277-5293.

Levi, S., 1975, Comparison of two methods of performing the Thellier experiment (or, how the Thellier experiment should not be done): Journal of Geomagnetism and Geoelectricity, v. 27, p. 245-255.

Levi, S., 1977, The effect of magnetite particle size on paleointensity determinations of the geomagnetic field: Physics of the Earth and Planetary Interiors, v. 13, p. 245-259.

Mankinen, E.A., and Champion, D.E., 1993*a*, Broad trends in geomagnetic paleointensity on Hawaii during Holocene time: Journal of Geophysical Research, v. 98, p. 7959-7976.

Mankinen, E.A., and Champion, D.E., 1993*b*, Latest Pleistocene and Holocene geomagnetic paleointensity on Hawaii: Science, v. 262, p. 412-416.

Mankinen, E.A., Prévot, M., Grommé, C.S., and Coe, R.S., 1985, The Steens Mountain (Oregon) geomagnetic polarity transition, 1. Directional history, duration of episodes, and rock magnetism: Journal of Geophysical Research, v. 90, p. 10,393-10,416.

Mankinen, E.A., Grommé, C.S., Dalrymple, G.B., Lanphere, M.A., and Bailey, R.A., 1986, Paleomagnetism and K-Ar ages of volcanic rocks from Long Valley caldera, California: Journal of Geophysical Research, v. 91, p. 633-652.

Mazaud, A., Laj, C., and Bender, M., 1994, A geomagnetic chronology for Antarctic ice accumulation: Geophysical Research Letters, v. 21, p. 337-340.

Mazaud, A., Laj, C., Bard, E., Arnold, M., and Tric, E., 1991, Geomagnetic field control of ^{14}C production over the last 80 KY -- Implications for the radiocarbon time-scale: Geophysical Research Letters, v. 18, p. 1885-1888.

McElhinny, M.W., and Senanayake, W.E., 1982, Variations in the geomagnetic dipole, 1, The past 50,000 years: Journal of Geomagnetism and Geoelectricity, v. 34, p. 39-51.

Meynadier, L., Valet, J.-P., Weeks, R., Shackleton, N.J., and Hagee, V.L., 1992, Relative geomagnetic intensity of the field during the last 140 ka: Earth and Planetary Science Letters, v. 114, p. 39-57.

Nagata, T., Arai, Y., and Momose K., 1963, Secular variation of the geomagnetic total force during the last 5000 years: Journal of Geophysical Research, v. 68, p. 5277-5282.

Otake, H., Tanaka, H., Kono, M., and Saito, K., 1993, Paleomagnetic study of Pleistocene lavas and dikes of the Zao Volcanic Group, Japan: Journal of Geomagnetism and Geoelectricity, v. 45, p. 595-612.

Phillips, F.M., Zreda, M.G., Smith, S.S., Elmore, D., Kubik, P.W., and Sharma, P., 1990, Cosmogenic chlorine-36 chronology for glacial deposits at Bloody Canyon, eastern Sierra Nevada: Science, v. 248, p. 1529-1532.

Prévot, M., Mankinen, E.A., Coe, R.S., and Grommé, C.S., 1985, The Steens Mountain (Oregon) geomagnetic polarity transition, 2. Field intensity variations and discussion of reversal models: Journal of Geophysical Research, v. 90, p. 10,417-10,448.

Shaw, J., 1974, A new method of determining the magnitude of the palaeomagnetic field -- application to five historic lavas and five archaeological samples: Geophysical Journal of the Royal Astronomical Society, v. 39, p. 133-141.

Smith, P.J., 1967, The intensity of the ancient geomagnetic field -- A review and analysis: Geophysical Journal of the Royal Astronomical Society, v. 12, p. 321-362.

Sternberg, R.S., 1989, Archaeomagnetic paleointensity in the American Southwest during the past 2000 years: Physics of the Earth and Planetary Interiors, v. 56, p. 1-17.

Stuiver, M., Kromer, B., Becker, B., and Ferguson, C.W., 1986, Radiocarbon age calibration back to 13,300 years BP and the ^{14}C age matching of the German oak and US bristlecone pine chronologies: Radiocarbon, v. 28, p. 969-979.

Tanaka, H., Otsuka, A., Tachibana, T., and Kono, M., 1994, Paleointensities for 10-22 ka from volcanic rocks in Japan and New Zealand: Earth and Planetary Science Letters, v. 122, p. 29-42.

Thellier, E., and Thellier, O., 1959, Sur l'intensité du champ magnétique terrestre dans le passé historique et géologique: Annales de Géophysique, t. 15, p. 285-376.

Tric, E., Valet, J.-P., Gillot, P.-Y., and Lemeur, I., 1994, Absolute paleointensities between 60 and 160 kyear BP from Mount Etna (Sicily): Physics of the Earth and Planetary Interiors, v. 85, p. 113-129.

Tric, E., Valet, J.-P., Tucholka, P., Parterne, M., Labeyrie, L., Guichard, F., Tauxe, L., and Fontune, M., 1992, Paleointensity of the geomagnetic field during the last eighty thousand years: Journal of Geophysical Research, v. 97, p. 9337-9351.